

# Nuclear rainbow of the symmetric nucleus-nucleus system: Interchange of the nearside and farside scattering

Nguyen Tri Toan Phuc,<sup>1,2</sup> Nguyen Hoang Phuc,<sup>3,\*</sup> and Dao T. Khoa<sup>4</sup>

<sup>1</sup>*Department of Nuclear Physics, Faculty of Physics and Engineering Physics,  
University of Science, Ho Chi Minh City 700000, Vietnam*

<sup>2</sup>*Vietnam National University, Ho Chi Minh City 700000, Vietnam*

<sup>3</sup>*Phenikaa Institute for Advanced Study (PIAS), Phenikaa University, Hanoi 12116, Vietnam*

<sup>4</sup>*Institute for Nuclear Science and Technology, VINATOM, Hanoi 122772, Vietnam*

Extensive elastic scattering data measured at energies around 10 to 20 MeV/nucleon for some light identical systems, like  $^{12}\text{C}+^{12}\text{C}$  and  $^{16}\text{O}+^{16}\text{O}$ , were shown to exhibit the nuclear rainbow pattern of broad Airy oscillations of the elastic scattering cross section at medium and large angles. Because of the identity of the scattered projectile and recoiled target, the smooth rainbow pattern at angles around and beyond  $\theta_{\text{c.m.}} \approx 90^\circ$  is strongly deteriorated by the boson exchange in the  $^{12}\text{C}+^{12}\text{C}$  and  $^{16}\text{O}+^{16}\text{O}$  systems at low energies. The exchange symmetry of two identical nuclei implies the Mott interference of the direct and exchange scattering amplitudes, which destroys the nuclear rainbow pattern. The nuclear rainbow features in the elastic scattering of two identical nuclei have been discussed so far based on the nearside-farside (NF) decomposition of the scattering amplitude given by an optical model calculation neglecting the projectile-target exchange symmetry. Moreover, the NF decomposition method was developed in the 1970s by Fuller for *nonidentical* dinuclear systems only, and the details of how the exchange symmetry of an *identical* system affects the evolution of nuclear rainbow remain unexplored. For this purpose, the Fuller method is generalized in the present work for the elastic scattering of two identical (spin-zero) nuclei, with the projectile-target exchange symmetry taken explicitly into account. The results obtained for elastic  $^{12}\text{C}+^{12}\text{C}$  and  $^{16}\text{O}+^{16}\text{O}$  scattering at low energies show that the exchange symmetry results in a symmetric interchange of the nearside and farside scattering patterns at angles passing through  $\theta_{\text{c.m.}} = 90^\circ$ , which requires a more subtle interpretation of nuclear rainbow. We found further that a similar NF interchange also occurs in a nonidentical nucleus-nucleus system with the core-core symmetry at low energies, where the elastic cross section at backward angles is due mainly to the elastic transfer of cluster or nucleon between two identical cores. This interesting effect is illustrated in the elastic  $^{16}\text{O}+^{12}\text{C}$  scattering at low energies where the elastic  $\alpha$  transfer between two  $^{12}\text{C}$  cores has been proven to enhance the elastic cross section at backward angles.

## I. INTRODUCTION

Elastic heavy-ion (HI) scattering is usually associated with strong absorption, with the scattering cross section displaying a typical diffraction pattern at forward angles and falling down rapidly at larger angles [1]. Such a diffraction pattern results mainly from the surface scattering of the incident wave, and it can be described by different choices of the optical potential (OP), illustrating the well-known ambiguity of the HI optical potential [1, 2]. However, many  $\alpha$ -nucleus and several light HI systems were found to be quite weakly absorbing, enabling the (refractive) nuclear rainbow pattern to appear at medium and large scattering angles [2, 3]. Such a rainbow pattern originates from the refraction of incident wave at smaller (sub-surface) impact parameters that shows up in the scattering cross section at larger angles if the absorption is weak (see Fig. 1). As a consequence, the observation of nuclear rainbow allows us to probe the nucleus-nucleus interaction at both the surface and sub-surface distances, and to determine the real nucleus-nucleus OP with much less ambiguity (see, e.g.,

the topical review [3] for more details).

To motivate the present study, we briefly recall the main features of the nuclear rainbow phenomenon. When the absorption is weak, the interference pattern of scattering waves attractively refracted by the target (serving as a nuclear liquid drop) turns out to be analogous to the interference of light rays refracted by a water droplet that causes the atmospheric rainbow. As schematically illustrated in Fig. 1, the trajectories incident at the sub-surface impact parameters are attractively refracted to the *far side* of the scattering center [4, 5], and the interference of the two subamplitudes of the farside scattering ( $f_{F>}$  and  $f_{F<}$ ) gives rise to a broad oscillation pattern of elastic scattering cross section, which is a microscopic replica of the Airy oscillation pattern of the refracted light rays of atmospheric rainbow [3, 6]. Thus, the key to identify a nuclear rainbow is the Airy oscillation of the farside cross section in elastic nucleus-nucleus scattering, especially, the first Airy minimum A1 followed by a shoulder-like bump in elastic scattering cross section at medium and large angles [3, 6, 7].

The farside scattering pattern can be revealed by decomposing the elastic scattering amplitude into the *internal* component that penetrates the Coulomb + centrifugal barrier into the interior of the real OP, and the *barrier* component that is reflected from the barrier [8, 9].

\* phuc.nguyenhoang@phenikaa-uni.edu.vn

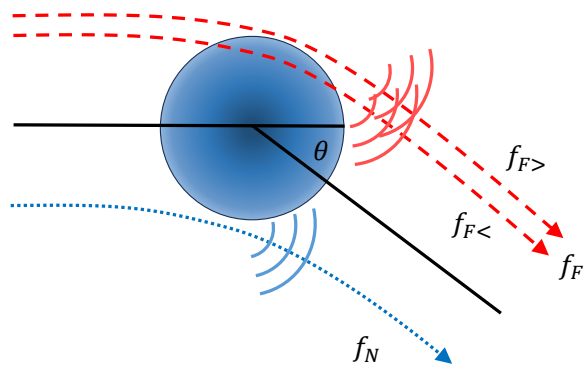


FIG. 1. Schematic view of trajectories of the incident wave scattered by nuclear OP at the surface and sub-surface impact parameters, to the nearside and farside of the scattering center, respectively.  $f_{F>}$  and  $f_{F<}$  are the farside subamplitudes with  $\ell > \ell_R$  and  $\ell < \ell_R$ , respectively, where  $\ell_R$  is the angular momentum at the rainbow point (see discussion in text).

A more popular, alternative interpretation of the farside scattering is based on the decomposition of the elastic scattering amplitude into the *nearside* and *farside* components, using the method originally developed by Fuller [10] which is referred to hereafter as the nearside-farside (NF) decomposition. The Airy oscillation pattern of the nuclear rainbow is formed by an interference of the outer ( $f_{F>}$ ) and inner ( $f_{F<}$ ) subamplitudes of the farside scattering. The  $f_{F>}$  and  $f_{F<}$  subamplitudes represent the contributions to the same scattering angle  $\theta$  of the (farside) partial waves with angular momenta  $\ell > \ell_R$  and  $\ell < \ell_R$ , respectively, where  $\ell_R$  is the angular momentum at the minimum of the deflection function, the *rainbow point* [11] that determines the corresponding rainbow angle  $\Theta_R$  in the observable angular range ( $0 < \Theta_R < 180^\circ$ ) [12]. The scattering to angles  $\theta > \Theta_R$ , i.e., to the dark side of the rainbow, is classically forbidden. The location of  $\Theta_R$  is shifting from large scattering angles at low energies to medium angles of  $\Theta_R \sim 40^\circ - 60^\circ$  at energies approaching Fermi domain of around 20 MeV/nucleon, where pronounced nuclear rainbow patterns have been observed [3]. It is complementary to note that  $\Theta_R \approx 138^\circ$  for the refracted light rays of atmospheric rainbow [4]. In elastic HI scattering, the  $f_{F<}$  subamplitude of the farside scattering is often suppressed by the absorption, and the Airy oscillation pattern of nuclear rainbow disappears. Therefore, a weak absorption is a prerequisite for the formation and observation of nuclear rainbow.

As mentioned above, the observation of the (refractive) nuclear rainbow pattern provides an important database for studies of the nucleus-nucleus interaction at low and medium energies [2, 3]. Because a nuclear rainbow is formed mainly by the farside trajectories refracted by a strongly attractive nucleus-nucleus OP, the nuclear rainbow pattern is absent in elastic electron-nucleus or nucleon-nucleus scattering where the scattering potential

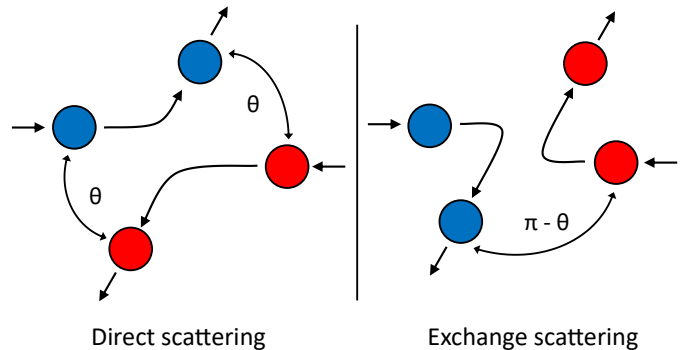


FIG. 2. Kinematical illustration of the direct and exchange scattering of two identical nuclei.

is not attractive enough to give rise to the farside scattering [6]. Thus, the nuclear rainbow can appear only in the refractive  $\alpha$ -nucleus or nucleus-nucleus scattering which is governed by the deep attractive real OP [3].

The nuclear rainbow pattern has been shown mainly so far by using the Fuller decomposition method [10]. However, this method was formulated for a *nonidentical* dinuclear system only, and it remains unexplored how the projectile-target exchange symmetry of an *identical* system affects the nuclear rainbow pattern. For this purpose, we have generalized in the present work, the Fuller method for the elastic scattering of two identical (even-even) nuclei, taking into account exactly the projectile-target exchange symmetry. The generalized method is then used to study the nuclear rainbow pattern in elastic  $^{12}\text{C}+^{12}\text{C}$  and  $^{16}\text{O}+^{16}\text{O}$  scattering, which was proven to be strongly refractive [3, 13–18].

Because of the identity of two nuclei, the detector cannot distinguish between the scattered projectile (in the direct scattering) and recoiled target (in the exchange scattering) as illustrated in Fig. 2, and the total scattering wave function of an identical nucleus-nucleus system must be composed of both the direct and exchange components. Then, the total wave function becomes symmetric or antisymmetric with respect to the projectile-target exchange [19] for the integer or half-integer nuclear spin, respectively,

$$\Psi_{\text{total}}(\mathbf{r}) \sim [\Psi(\mathbf{r}) \pm \Psi(-\mathbf{r})], \quad \mathbf{r} = \mathbf{r}_1 - \mathbf{r}_2. \quad (1)$$

As a result, the total elastic scattering (ES) amplitude is also symmetric or antisymmetric in the same manner, with respect to the projectile-target exchange [12]

$$f_{\text{ES}}(\theta) = f_{\text{Mott}}(\theta) + f(\theta) \pm f(\pi - \theta), \quad \theta \equiv \theta_{\text{c.m.}} \quad (2)$$

where  $f_{\text{Mott}}(\theta)$  is the *Coulomb* scattering amplitude of two identical ions, known as the Mott scattering amplitude [19],  $f(\theta)$  and  $f(\pi - \theta)$  are the direct and exchange *nuclear* scattering amplitudes. The symmetrization or antisymmetrization procedure (2) is commonly available in different OM or coupled-channel codes [20–22].

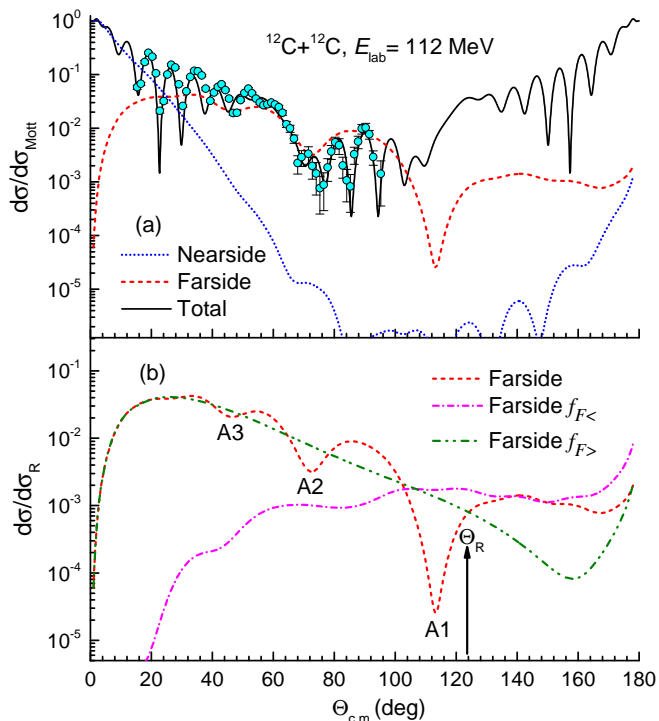


FIG. 3. (a) Elastic  $^{12}\text{C}+^{12}\text{C}$  scattering data measured at  $E_{\text{lab}} = 112$  MeV [23] in comparison with the OM results, taking explicitly into account the boson symmetrization (1)-(2) of two identical  $^{12}\text{C}$  nuclei (solid line). The nearside (dotted line) and farside (dashed line) cross sections were obtained from the NF decomposition (3)-(6) of the elastic scattering amplitude, neglecting the projectile-target symmetry. (b) The full farside cross section (dashed line) and cross sections given by  $f_{F>}$  (dashed dotted dotted line) and  $f_{F<}$  (dashed dotted line) farside subamplitudes.  $A_k$  is the  $k$ -order Airy minimum, and  $\Theta_R$  is the rainbow angle determined from the minimum of the deflection function [12].

A typical example is the elastic  $^{12}\text{C}+^{12}\text{C}$  scattering data measured at  $E_{\text{lab}} = 112$  MeV shown in Fig. 3, which can be properly described only when the projectile-target exchange symmetry (2) is taken into account in the OM calculation. So far, the nuclear rainbow pattern in elastic  $^{12}\text{C}+^{12}\text{C}$  scattering has been studied only qualitatively with the projectile-target exchange symmetry (2) turned off in the OM calculation, and the standard (unsymmetrized) NF decomposition [10] of the elastic scattering amplitude could be made to reveal the Airy oscillation of the farside cross section. One can see in panel (b) of Fig. 3 that such an Airy oscillation is given by an interference of the two subamplitudes of the farside scattering. The outer  $f_{F>}(\theta)$  and inner  $f_{F<}(\theta)$  subamplitudes were determined in this work based on the method suggested by McVoy *et al.* [11]. However, the broad Airy oscillation of the (unsymmetrized) farside cross section from the rainbow angle  $\Theta_R \approx 123^\circ$ , over A1 and A2 to medium angles, is strongly distorted when the projectile-target symmetrization is taken explicitly into account as

shown in panel (a) of Fig. 3, and the elastic scattering cross section becomes symmetric with respect to the angular exchange  $\theta \leftrightarrow \pi - \theta$ . It is also obvious from the exchange symmetry that the quickly oscillating pattern at the most backward angles is due to a NF interference similar to that established at forward angles, but the original Fuller method [10] is not appropriate for that kind of NF analysis. In fact, a proper determination of the nearside and farside scattering amplitudes for a symmetric nucleus-nucleus system remains an unsolved problem.

## II. NF DECOMPOSITION OF THE ELASTIC SCATTERING AMPLITUDE OF TWO IDENTICAL SPIN-ZERO NUCLEI

We briefly recall how the nuclear rainbow pattern is revealed by decomposing the elastic scattering amplitude into the nearside  $f^{(N)}$  and farside  $f^{(F)}$  components using Fuller method [10]. By splitting the Legendre function  $P_\ell(\cos\theta)$  into two waves scattered at  $\theta$  but running in the opposite directions around the scattering center, the NF components of the unsymmetrized (nuclear) elastic scattering amplitude is obtained as

$$f(\theta) = f^{(N)}(\theta) + f^{(F)}(\theta), \quad (3a)$$

$$f^{(N)}(\theta) = \frac{i}{2k} \sum_{\ell} (2\ell + 1) B_{\ell} \tilde{Q}_{\ell}^{(-)}(\cos\theta), \quad (3b)$$

$$f^{(F)}(\theta) = \frac{i}{2k} \sum_{\ell} (2\ell + 1) B_{\ell} \tilde{Q}_{\ell}^{(+)}(\cos\theta). \quad (3c)$$

The partial-wave amplitude  $B_{\ell}$  is determined as

$$B_{\ell} = \exp(2i\sigma_{\ell})(1 - S_{\ell}), \quad (4)$$

where  $\sigma_{\ell}$  is the Coulomb phase shift, and  $S_{\ell}$  is the scattering  $S$  matrix element for the  $\ell$ -th partial wave. The traveling wave components are

$$\tilde{Q}_{\ell}^{(\mp)}(\cos\theta) = \frac{1}{2} \left[ P_{\ell}(\cos\theta) \pm \frac{2i}{\pi} Q_{\ell}(\cos\theta) \right], \quad (5)$$

where  $Q_{\ell}(\cos\theta)$  is the Legendre function of the second kind. A nice feature of the quantal scattering theory is that the wave associated with  $Q_{\ell}^{(-)}(\cos\theta)$  is deflected from the *near side* of the scattering center to angle  $\theta$ , and that associated with  $Q_{\ell}^{(+)}(\cos\theta)$  is deflected from the opposite, *far side* of the scattering center to the same angle  $\theta$ . Thus, the nearside amplitude  $f^{(N)}(\theta)$  accounts mainly for the *repulsively* diffracted wave that scatters at the surface, and the farside amplitude  $f^{(F)}(\theta)$  accounts for the *attractively* refracted wave that penetrates more into the sub-surface of the target nucleus, as schematically shown in Fig. 1.

Because of the short range of the strong interaction, the NF decomposition of the *nuclear* scattering amplitude (3) can be done numerically, with the nuclear nearside and farside amplitudes merging naturally at  $\theta = 0$

and  $\theta = \pi$ . However, the long-range Coulomb interaction poses a technical difficulty for the NF decomposition of the *Coulomb* scattering amplitude based on the partial wave expansion (3). Moreover, the Coulomb scattering amplitude is singular at  $\theta = 0$ , where the partial wave series diverges. By projecting argument of the Legendre function into the complex plane, Fuller managed to treat the singularity at  $\theta = 0$  and obtained the NF components  $f_R^{(N)}(\theta)$  and  $f_R^{(F)}(\theta)$  of the Rutherford scattering amplitude [10] as

$$f_R^{(N)}(\theta) = f_R(\theta) \left\{ \frac{-iS(\theta)}{2\pi} [\sin^2(\theta/2)]^{1+i\eta} + 1 - e^{2\pi\eta} \right\}, \quad (6a)$$

$$f_R^{(F)}(\theta) = f_R(\theta) \left\{ \frac{iS(\theta)}{2\pi} [\sin^2(\theta/2)]^{1+i\eta} - \frac{e^{-2\pi\eta}}{1 - e^{2\pi\eta}} \right\}. \quad (6b)$$

$$f_R(\theta) = -\frac{\eta}{2ik \sin^2(\theta/2)} \exp [2i\sigma_0 - i\eta \ln \sin^2(\theta/2)], \quad (6c)$$

$$S(\theta) = (1 + i\eta)^{-1} F(1, 1 + i\eta; 2 + i\eta; \sin^2(\theta/2)), \quad (6d)$$

and hypergeometric function

$$\begin{aligned} F(a, b; c; z) &= {}_2F_1(a, b; c; z), \\ &= \frac{\Gamma(c)}{\Gamma(a)\Gamma(b)} \sum_{n=0}^{\infty} \frac{\Gamma(a+n)\Gamma(b+n)}{\Gamma(c+n)} \frac{z^n}{n!}. \end{aligned} \quad (6e)$$

Here  $k$  and  $\eta$  are the wave number and Sommerfeld parameter, respectively, and  $\sigma_0 = \arg \Gamma(1 + i\eta)$  [19].

As discussed above, the elastic scattering cross section of two identical (spin-zero) nuclei is symmetric about  $\theta = \pi/2$ . In particular, the Coulomb scattering amplitude of two identical ions is known as the Mott scattering amplitude [19], which is determined in this case from the Rutherford scattering amplitude (6b) as

$$f_{\text{Mott}}(\theta) = f_R(\theta) + f_R(\pi - \theta). \quad (7)$$

After some trigonometric transformation, we obtain

$$f_{\text{Mott}}(\theta) = f_R(\pi) \left[ \left( \frac{1-x}{2} \right)^{-1-i\eta} + \left( \frac{1+x}{2} \right)^{-1-i\eta} \right], \quad (8)$$

where  $x = \cos \theta$ . Applying the Fuller technique, we have projected the Mott scattering amplitude (7)-(8) into the complex plane, also in terms of the two components (in the forward and backward scattering angles [10]). After a lengthy analytical transformation, the nearside and farside components of the Mott scattering amplitude can be rigorously expressed in terms of those of the Rutherford amplitude (6a)-(6b) as

$$f_{\text{Mott}}^{(N)}(\theta) = f_R^{(N)}(\theta) + f_R^{(F)}(\pi - \theta), \quad (9)$$

$$f_{\text{Mott}}^{(F)}(\theta) = f_R^{(F)}(\theta) + f_R^{(N)}(\pi - \theta). \quad (10)$$

Thus, the nearside component (9) of the Mott amplitude is a superposition of the nearside and farside components of the Rutherford amplitude determined at the angles  $\theta$  and  $\pi - \theta$ , respectively. Similarly, the farside component (10) is a superposition of the farside and nearside components of the Rutherford amplitude determined at the angles  $\theta$  and  $\pi - \theta$ , respectively.  $f_{\text{Mott}}^{(N)}(\theta)$  and  $f_{\text{Mott}}^{(F)}(\theta)$  become equal at  $\theta = \pi/2$ .

The symmetrization of the nuclear scattering amplitude is straightforwardly based on the partial wave series (3), and the symmetrized amplitude can be decomposed into the nearside and farside components as

$$\begin{aligned} f_{\text{sym}}(\theta) &= f_{\text{sym}}^{(N)}(\theta) + f_{\text{sym}}^{(F)}(\theta) \\ &= \frac{1}{2ik} \sum_{\ell} B_{\ell} [1 + (-1)^{\ell}] \left[ \tilde{Q}_{\ell}^{(-)}(\cos \theta) + \tilde{Q}_{\ell}^{(+)}(\cos \theta) \right], \end{aligned} \quad (11)$$

where the summation is done over the *even* partial waves  $\ell$  only. Given  $(-1)^{\ell} \tilde{Q}_{\ell}^{(\pm)}(\cos \theta) = \tilde{Q}_{\ell}^{(\mp)}(\cos(\pi - \theta))$ , the nearside and farside components of the symmetrized nuclear amplitude (11) are readily obtained as

$$f_{\text{sym}}^{(N)}(\theta) = f_{\text{sym}}^{(N)}(\theta) + f_{\text{sym}}^{(F)}(\pi - \theta), \quad (12)$$

$$f_{\text{sym}}^{(F)}(\theta) = f_{\text{sym}}^{(F)}(\theta) + f_{\text{sym}}^{(N)}(\pi - \theta), \quad (13)$$

where  $f^{(N,F)}$  are the nearside and farside components of the unsymmetrized nuclear scattering amplitude (3b)-(3c). Thus, exactly in the same way as for the Mott scattering amplitude, the nearside component of the symmetrized nuclear scattering amplitude (11) is also a superposition of the nearside and farside components of the unsymmetrized nuclear amplitude (3a) summed over the even partial waves  $\ell$  at the angles  $\theta$  and  $\pi - \theta$ , respectively, and vice versa for the farside component (11).

It is helpful to express explicitly the total ES amplitude of two identical (spin zero) nuclei in terms of the direct (D) and exchange (EX) scattering amplitudes, as illustrated in Fig. 2,

$$f_{\text{ES}}(\theta) = f_{\text{D}}(\theta) + f_{\text{EX}}(\pi - \theta), \quad (14)$$

where

$$f_{\text{D}}(\theta) = f_R(\theta) + f(\theta), \quad (15a)$$

$$f_{\text{EX}}(\pi - \theta) = f_R(\pi - \theta) + f(\pi - \theta). \quad (15b)$$

It is easy to deduce from Eqs. (14)-(15) the symmetric interchange of the direct and exchange scattering amplitudes  $f_{\text{D}} \rightleftharpoons f_{\text{EX}}$  with the scattering angle passing through  $\theta = 90^\circ$ . Combining the nearside and farside components of the Mott (9)-(10) and nuclear (12)-(13) scattering amplitudes, we can express the nearside and farside components of the ES amplitude as

$$f_{\text{ES}}^{(N)}(\theta) = f_{\text{D}}^{(N)}(\theta) + f_{\text{EX}}^{(F)}(\pi - \theta), \quad (16)$$

$$f_{\text{ES}}^{(F)}(\theta) = f_{\text{D}}^{(F)}(\theta) + f_{\text{EX}}^{(N)}(\pi - \theta). \quad (17)$$

In the same way, one can deduce from Eqs. (16)-(17) the symmetric interchange of the *nearside* and *farside* components of the total ES amplitude  $f_{\text{ES}}^{(N)} \rightleftharpoons f_{\text{ES}}^{(F)}$  as the scattering angle passes through  $90^\circ$ . Because the direct NF cross sections become negligible at angles  $\theta > 90^\circ$  (see Fig. 3), we obtain from Eqs. (16)-(17)

$$f_{\text{ES}}^{(N)}(\theta) \approx f_{\text{EX}}^{(F)}(\pi - \theta) \text{ at } \theta > 90^\circ, \quad (18)$$

$$f_{\text{ES}}^{(F)}(\theta) \approx f_{\text{EX}}^{(N)}(\pi - \theta) \text{ at } \theta > 90^\circ. \quad (19)$$

Thus, the symmetric interchange of the nearside and far-side scattering patterns in the elastic scattering of two identical nuclei is caused naturally by the projectile-target exchange symmetry. As shown in the next section, such a NF interchange implies a more subtle interpretation of nuclear rainbow over the whole angular range for the considered symmetric systems.

### III. RESULTS FOR THE ELASTIC $^{12}\text{C}+^{12}\text{C}$ AND $^{16}\text{O}+^{16}\text{O}$ SCATTERING

We present here the results of the NF decomposition of elastic  $^{12}\text{C}+^{12}\text{C}$  and  $^{16}\text{O}+^{16}\text{O}$  scattering at low energies, where the data were measured accurately up to angles around and beyond  $\theta \approx 90^\circ$ . The real OP is given by the double-folding calculation [18] using the CDM3Y3 density-dependent interaction [16], and the imaginary OP is parametrized in the Woods-Saxon (WS) form to tailor the weak absorption of these systems. A slight renormalization  $N_R$  of the real folded potential and WS parameters are obtained from the best OM fit to the measured data using the code ECIS97 [20]. Very prominent are the  $^{12}\text{C}+^{12}\text{C}$  scattering data measured by Stokstad *et al.* [23] at low energies, which cover a wide angular range. Based on these data, a realistic OM description of the nuclear rainbow pattern and  $90^\circ$  excitation function was obtained by McVoy and Brandan [14], with the angular location of Airy minima at different energies (the famous Airy elephant discussed in Ref. [14]).

The OM results for elastic  $^{12}\text{C}+^{12}\text{C}$  scattering at  $E_{\text{lab}} = 112$  and 121.6 MeV are shown in Figs. 3-4. The NF decomposition of the *unsymmetrized* ES amplitude gives the first Airy minimum A1 located at  $\theta \lesssim 100^\circ$  (see Fig. 3), which is destroyed by the projectile-target symmetrization (2). The impact of the projectile-target exchange symmetry is shown in Fig. 4, where the NF decomposition of the *symmetrized* ES amplitude was done using Eqs. (16)-(17). While the ES cross section is symmetric about the angle  $\theta = 90^\circ$ , the nearside and far-side scattering cross sections at angles  $\theta < 90^\circ$  are symmetrically interchanged to the far-side and nearside scattering cross sections at angles  $\theta > 90^\circ$ , respectively. We note two interesting effects that can be deduced from Fig. 4:

i) The Airy pattern not destroyed by the symmetrization of the direct and exchange scattering amplitudes is reflected symmetrically about  $\theta = 90^\circ$ , and each Airy minimum located in the (direct) far-side cross section at

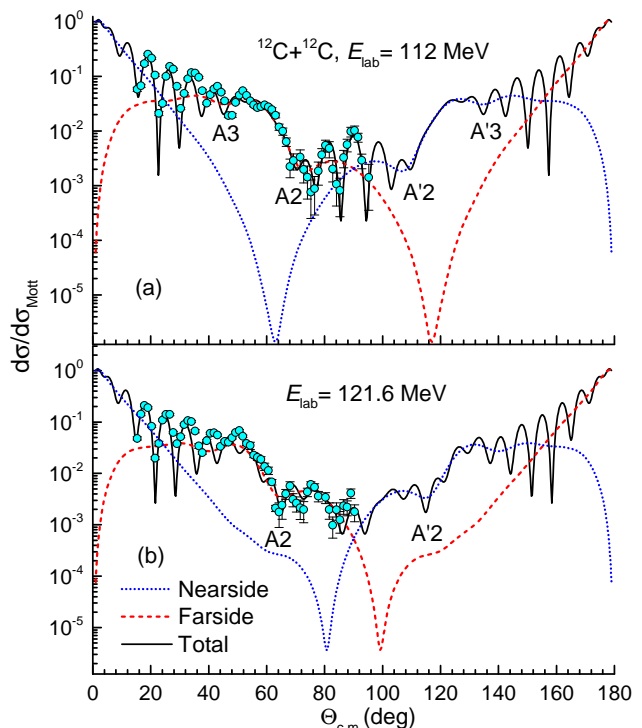


FIG. 4. (a) Elastic  $^{12}\text{C}+^{12}\text{C}$  scattering data measured at  $E_{\text{lab}} = 112$  MeV [23] in comparison with results of the OM calculation, taking exactly into account the projectile-target symmetrization (solid line). The nearside (dotted line) and far-side (dashed line) cross sections were given by the NF decomposition (16)-(17) of the ES amplitude.  $Ak$  and  $A'k$  are the  $k$ -order Airy minimum of the direct far-side cross section at  $\theta$  and its symmetric partner of the exchange far-side cross section at  $\pi - \theta$ , respectively.

(b) The same as (a) but for the elastic  $^{12}\text{C}+^{12}\text{C}$  scattering data measured at  $E_{\text{lab}} = 121.6$  MeV [23].

angle  $\theta < 90^\circ$  has its symmetric partner located in the (exchange) far-side cross section at angle  $\pi - \theta$ . For strong refractive systems such as those considered here, the NF cross sections exhibit a distinct symmetric Airy minima pattern resembling “butterfly wings”.

ii) The interference pattern at angles around  $90^\circ$  can be interpreted as the interference of the nearside and far-side components of the total ES amplitude. However, such a NF interference of the total ES amplitude is in fact the interference of two far-side amplitudes (the direct and exchange ones).

The OM results for the elastic  $^{16}\text{O}+^{16}\text{O}$  scattering at  $E_{\text{lab}} = 124$  and 145 MeV are shown in Fig. 5, and one observes the same “butterfly-wings” Airy pattern that is symmetric about  $\theta = 90^\circ$  due to the projectile-target exchange symmetry. We note that the refractive, nuclear rainbow pattern was well established in elastic  $^{12}\text{C}+^{12}\text{C}$  and  $^{16}\text{O}+^{16}\text{O}$  scattering at higher energies, like the prominent primary rainbow observed for the  $^{16}\text{O}+^{16}\text{O}$  system at  $E_{\text{lab}} = 350$  MeV [24, 25]. However, as energy increases, the broad Airy pattern of the

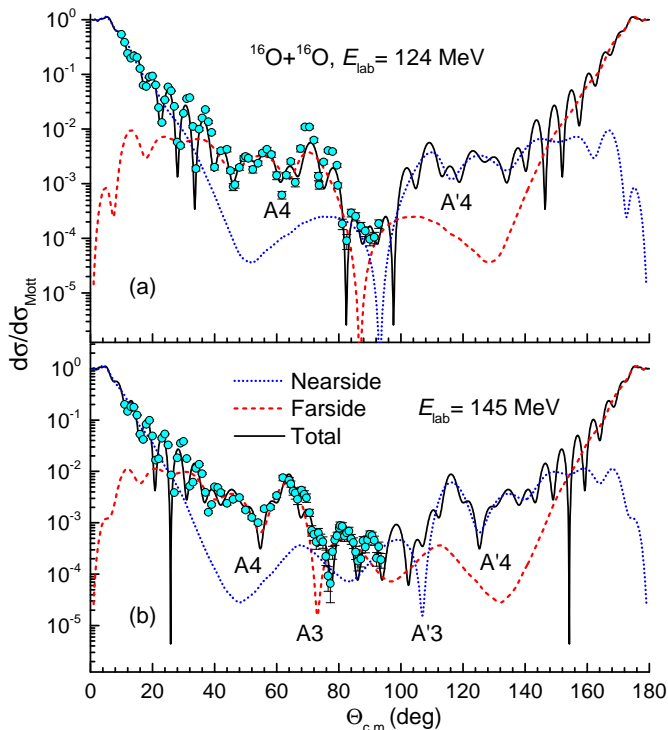


FIG. 5. The same as Fig. 4 but for the elastic  $^{16}\text{O}+^{16}\text{O}$  scattering data measured at  $E_{\text{lab}} = 124$  MeV [26] (a), and 145 MeV [27] (b).

farside cross section is shifted to smaller angles, and the ES cross section at angles around  $90^\circ$  merges deeply into the dark side of nuclear rainbow and is, therefore, too small to be measurable. Therefore, the low-energy elastic  $^{12}\text{C}+^{12}\text{C}$  and  $^{16}\text{O}+^{16}\text{O}$  data [23, 26, 27] are very valuable for the study of the projectile-target exchange symmetry of these identical systems.

As pointed out in ii), the oscillation pattern of the elastic cross section around  $\theta = 90^\circ$  is resulted from an interference of two farside amplitudes, the direct and exchange ones, which are generated by the same OP. Therefore, the ES cross section at  $\theta$  around  $90^\circ$  is expected to be particularly sensitive to the real OP at sub-surface distances, which would help to determine the real OP with less ambiguity [3].

We have explored such a sensitivity to the real OP of the elastic  $^{12}\text{C}+^{12}\text{C}$  data measured at  $E_{\text{lab}} = 112$  MeV by slightly rescaling the strength of the best-fit real folded OP up and down by  $\approx 7\%$ , with the depth of the WS imaginary OP being adjusted in each case by  $\chi^2$  fit to the measured data. The radial shapes of the complex  $^{12}\text{C}+^{12}\text{C}$  OP are shown in Fig. 6, and the corresponding OM results are compared with the data in Fig. 7. It can be seen in panel (b) of Fig. 7 that the Airy pattern of the (direct) farside scattering cross section is very sensitive to the strength of the real OP. The rescaling of the real OP shown in Fig. 6 results in different locations of the Airy minima of the direct farside cross section, which strongly

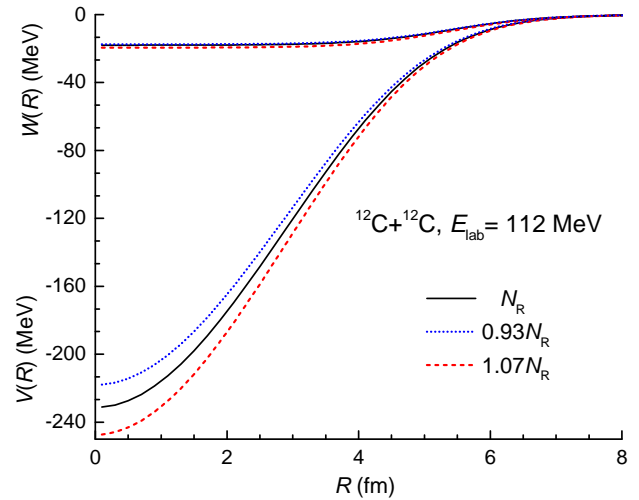


FIG. 6. Radial shapes of the real double-folded potential  $V$  rescaled up and down by around 7% from that given by the best-fit  $N_R \approx 1.177$ , and the corresponding WS imaginary potential of the total OP for the  $^{12}\text{C}+^{12}\text{C}$  system at  $E_{\text{lab}} = 112$  MeV.

affect the interference of the direct and exchange farside amplitudes at angles around  $90^\circ$ , as shown in panel (a) of Fig. 7. Similar sensitivity of the elastic  $^{12}\text{C}+^{12}\text{C}$  scattering data at  $E_{\text{lab}} = 78$  MeV [23] to the real OP was used in a recent study of the  $^{12}\text{C}+^{12}\text{C}$  fusion [28] to probe different treatments of the nuclear overlap density in the double-folding calculation of the real OP of the  $^{12}\text{C}+^{12}\text{C}$  system at astrophysical energies.

In summary, we have applied the newly developed NF decomposition method for the ES amplitude of two identical nuclei to show the effects caused by the projectile-target exchange symmetry to the nuclear rainbow pattern in elastic  $^{12}\text{C}+^{12}\text{C}$  and  $^{16}\text{O}+^{16}\text{O}$  scattering at low energies.

#### IV. ELASTIC $^{16}\text{O}+^{12}\text{C}$ SCATTERING AND THE CORE-CORE EXCHANGE EFFECT

A similar interchange of the NF scattering as that found above for the identical  $^{12}\text{C}+^{12}\text{C}$  and  $^{16}\text{O}+^{16}\text{O}$  systems might also be seen in a nonidentical system that has the core-core symmetry. We focus here on the  $^{16}\text{O}+^{12}\text{C}$  system that was considered as a good candidate for the observation of nuclear rainbow [29, 30]. Several experiments were carried out to measure elastic  $^{16}\text{O}+^{12}\text{C}$  scattering with high precision at low and medium energies, covering a wide angular range. We mention here elastic  $^{16}\text{O}+^{12}\text{C}$  data measured by the Kurchatov group [31–34] and Strasbourg group [35].

Different OM studies of elastic  $^{16}\text{O}+^{12}\text{C}$  scattering (see, e.g., [18, 31, 32]) have shown unambiguously the nuclear rainbow pattern of a broad Airy oscillation of the farside cross section. However, at low energies ( $E_{\text{lab}} \lesssim$

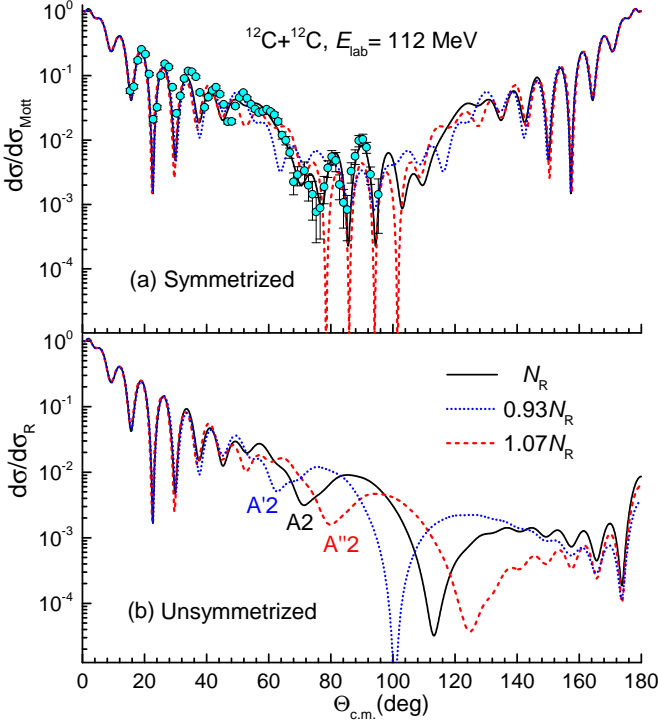


FIG. 7. (a) Elastic  $^{12}\text{C}+^{12}\text{C}$  data measured at  $E_{\text{lab}} = 112$  MeV [23] in comparison with the OM results given by the real folded OP rescaled up and down by around 7% from that given by the best-fit  $N_R \approx 1.177$  as shown in Fig. 6. (b) Results of the *unsymmetrized* OM calculation using three choices of the real OP, which result in three different locations of the second Airy minimum A2 of the (direct) farside cross section.

132 MeV) the broad pattern of Airy oscillation is destroyed by a quick oscillation of elastic  $^{16}\text{O}+^{12}\text{C}$  cross section at backward angles. Such a distortion of nuclear rainbow is due mainly to the elastic  $\alpha$  transfer (ET) between two  $^{12}\text{C}$  cores as illustrated in Fig. 8 (see, e.g., Refs. [36–40]). Recent coupled reaction channel (CRC) studies of elastic  $^{16}\text{O}+^{12}\text{C}$  scattering, taking into account the coupling between the ES and ET channels [38, 39] have shown that the ET process significantly enhances the nearside cross section at backward angles, indicating that an interchange of the NF scattering seems to take place in elastic  $^{16}\text{O}+^{12}\text{C}$  scattering.

Because of two identical  $^{12}\text{C}$  cores, the ES channel  $^{12}\text{C}(^{16}\text{O}, ^{16}\text{O})^{12}\text{C}$  and ET channel  $^{12}\text{C}(^{16}\text{O}, ^{12}\text{C})^{16}\text{O}$  have the same final state which is indistinguishable for the detector (see Fig. 8). As a result, the total (nonlocal) wave function of the  $^{16}\text{O}+^{12}\text{C}$  system is composed of both the ES and ET components, with prime indicating the relative coordinate in the ET channel [22]

$$\Psi_{\text{total}}(\mathbf{r}, \mathbf{r}') \sim [\Psi_{\text{ES}}(\mathbf{r}) + \Psi_{\text{ET}}(-\mathbf{r}')],$$

where  $\mathbf{r} = \mathbf{r}_1 - \mathbf{r}_2$ ,  $\mathbf{r}' = \mathbf{r}'_1 - \mathbf{r}'_2$ .

Like the total ES amplitude of two identical nuclei (14), the total elastic amplitude of the  $^{16}\text{O}+^{12}\text{C}$  system can

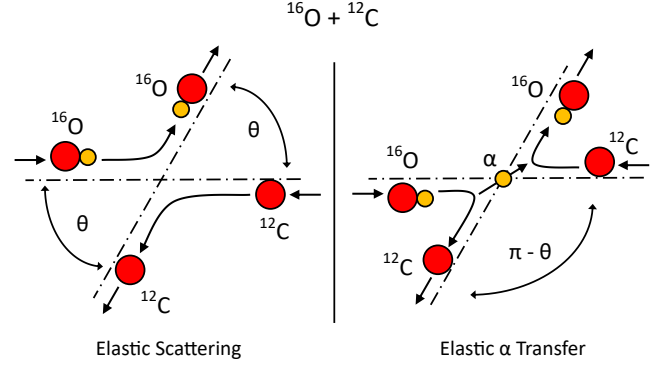


FIG. 8. Kinematical illustration of the elastic scattering and elastic  $\alpha$  transfer processes in the  $^{16}\text{O}+^{12}\text{C}$  system.

be expressed as a coherent sum of the ES amplitude at  $\theta$  and ET amplitude at  $\pi - \theta$  [41–44]

$$f_{\text{total}}(\theta) = f_{\text{R}}(\theta) + f(\theta) + f_{\text{ET}}(\pi - \theta) = f_{\text{ES}}(\theta) + f_{\text{ET}}(\pi - \theta), \quad (20)$$

where  $f_{\text{ES}}$  and  $f_{\text{ET}}$  are given by the CRC solutions obtained for the ES and ET channels, respectively [21, 41]. One can see from Eqs. (14) and (20) that  $f_{\text{ET}}(\pi - \theta)$  is analogous to  $f_{\text{EX}}(\pi - \theta)$  of the identical system. The ET amplitude can be expanded over a partial wave series as

$$f_{\text{ET}}(\pi - \theta) = \frac{1}{2ik} \sum_{\ell} (2\ell + 1) e^{2i\sigma_{\ell}} (-1)^{\ell} S_{\text{ET}}^{(\ell)} P_{\ell}(\cos \theta), \quad (21)$$

where  $S_{\text{ET}}^{(\ell)}$  is the elastic transfer  $S_{\text{ET}}$ -matrix element for the  $\ell$ -th partial wave. The total elastic amplitude (20) can then be expressed as

$$f_{\text{total}}(\theta) = f_{\text{R}}(\theta) + \frac{1}{2ik} \sum_{\ell} (2\ell + 1) e^{2i\sigma_{\ell}} \times [S_{\text{ES}}^{(\ell)} + (-1)^{\ell} S_{\text{ET}}^{(\ell)}] P_{\ell}(\cos \theta). \quad (22)$$

At variance with the total elastic scattering amplitude (9) of two identical nuclei, summation of the partial wave series (22) is done over both *odd* and *even* partial waves  $\ell$ , with the parity-dependent elastic  $\alpha$  transfer  $S_{\text{ET}}$  matrix added to the elastic scattering  $S_{\text{ES}}$  matrix. The interference of  $S_{\text{ES}}$  and  $S_{\text{ET}}$  leads to the oscillation of elastic  $^{16}\text{O}+^{12}\text{C}$  cross section observed at large angles (see Fig. 9). Schematically, the elastic  $\alpha$  transfer shown in Fig. 8 can also be treated as the core-core exchange that naturally leads to that interference.

In this work, the coupling between the ES and ET channels is taken explicitly into account by solving the two-channel CRC equations using the code FRESKO [21, 22], to obtain  $S_{\text{ES}}^{(\ell)}$  and  $S_{\text{ET}}^{(\ell)}$  separately for each partial wave. Although the final state of these two channels is the same, there is no way to link explicitly both  $S_{\text{ES}}$  and  $S_{\text{ET}}$  to the same  $^{16}\text{O}+^{12}\text{C}$  scattering potential as might naively be expected from a comparison

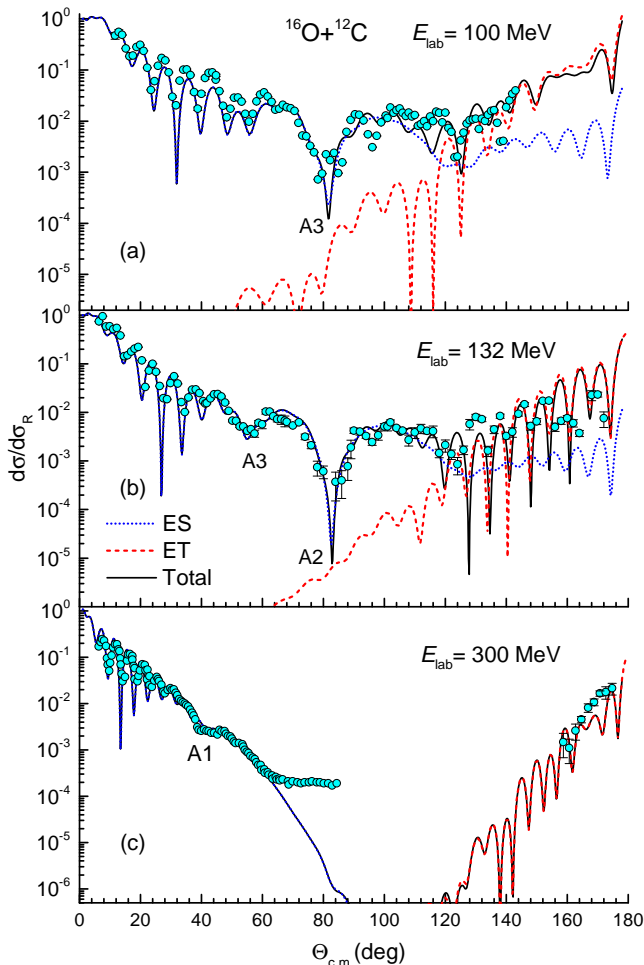


FIG. 9. Two-channel CRC description of elastic  $^{16}\text{O}+^{12}\text{C}$  data measured at  $E_{\text{lab}} = 100$  MeV (a), 132 MeV (b), and 300 MeV (c) [30–32, 35], using the real double-folded and WS imaginary OP. The ES, ET, and total (ES+ET) elastic cross sections are shown as dotted, dashed, and solid lines, respectively.

of Figs. 2 and 8. While  $S_{\text{ES}}$  is associated with elastic (Coulomb+nuclear) scattering,  $S_{\text{ET}}$  represents the elastic  $\alpha$  transfer between two  $^{12}\text{C}$  cores which is associated with the dissociation  $^{16}\text{O} \rightarrow \alpha + ^{12}\text{C}$ . Within the two-channel CRC formalism,  $S_{\text{ES}}$  and  $S_{\text{ET}}$  are determined separately using the  $^{16}\text{O}+^{12}\text{C}$  optical potential and the (nonlocal)  $\alpha$ -transfer interaction potential, respectively (we refer to Ref. [38] for further details). We note that in the one-channel OM study, one can effectively mimic the ET by adding an angular-momentum or parity dependent term to the  $^{16}\text{O}+^{12}\text{C}$  optical potential [41, 44]. In a similar manner, the ET can also be represented by a modified elastic scattering  $S$  matrix [42, 43] that contains an  $\ell$ -dependent component like that in Eq. (22).

The elastic  $^{16}\text{O}+^{12}\text{C}$  cross sections given by the total elastic amplitude (22) obtained from solutions of the two-channel CRC calculation are compared with elastic

$^{16}\text{O}+^{12}\text{C}$  data measured at  $E_{\text{lab}} = 100$  MeV [35], 132 MeV [31, 32], and 300 MeV [30] in Fig. 9, and one can see that the enhanced oscillating elastic cross sections at backward angles are mainly caused by the ET or the core-core exchange at these energies. Especially, the elastic  $^{16}\text{O}+^{12}\text{C}$  data measured at 300 MeV at the most backward angles are totally due to the ET as can be seen in panel (c) of Fig. 9. The good CRC description of elastic  $^{16}\text{O}+^{12}\text{C}$  data shown in Fig. 9 is obtained consistently at three energies with the  $\alpha$  spectroscopic factor  $S_{\alpha} \approx 1.96$ , in agreement with the earlier DWBA and two-channel CRC results [36, 45]. Although this  $S_{\alpha}$  value is larger than those predicted by the shell model (SM) [46] or  $\alpha$ -cluster model [47], it can be adopted as an effective  $S_{\alpha}$  factor for the description of the ET process in the two-channel CRC calculation. In fact, a more comprehensive CRC calculation of elastic  $^{16}\text{O}+^{12}\text{C}$  scattering, coupling up to 10 reaction channels of both direct and indirect (multistep)  $\alpha$  transfers [38], accounts well for elastic  $^{16}\text{O}+^{12}\text{C}$  data at backward angles using  $S_{\alpha}$  predicted by the SM calculation [46]. We note here that the (extended) continuum discretized coupled channel (CDCC) approach [48], including the core-core exchange into the nonlocal CDCC calculation of low-energy elastic  $^{16}\text{O}+^{12}\text{C}$  scattering, shows the same dominant contribution of the core-core exchange to elastic  $^{16}\text{O}+^{12}\text{C}$  cross section at large angles.

Note that the ES and ET contributions to the total elastic  $^{16}\text{O}+^{12}\text{C}$  cross section are not symmetrically equal as the direct and exchange scattering amplitudes found above for two identical nuclei. To explore this effect in more details, the NF decomposition of the elastic  $^{16}\text{O}+^{12}\text{C}$  amplitude, given by the two-channel CRC calculation at  $E_{\text{lab}} = 132$  MeV, has been done separately for the ES, ET, and total (ES+ET) elastic amplitude using Fuller’s method [10]. One can see in panel (b) of Fig. 10 that the ET cross section is *not* a symmetrically reflected pattern of the ES cross section shown in panels (a). While the ES cross section is dominated by the farside scattering over a wide angular range, the ET cross section is a typical NF interference pattern, which indicates a surface character of the ET between two  $^{12}\text{C}$  cores. This is natural because the contribution of  $f_{\text{ET}}(\pi - \theta)$  to  $f_{\text{total}}(\theta)$  at the most backward angles represents in fact the ET process occurring physically at the most forward angles.

At variance with the ES occurring at forward angles that includes both the Coulomb and nuclear scattering, the repulsive Coulomb interaction does not contribute to the ET process which occurs at backward angles. As a result, we found a significant *non-refractive* farside component of the ET cross section shown in panel (b) of Fig. 10. Although generated by the attractive nuclear interaction, such a farside cross section cannot be associated with nuclear rainbow due to a quick modulation of the ET farside cross section caused mainly by the diffraction of the  $\alpha$ -transfer wave.

Despite the difference discussed above for the ES and ET cross sections, the NF components of the total elastic



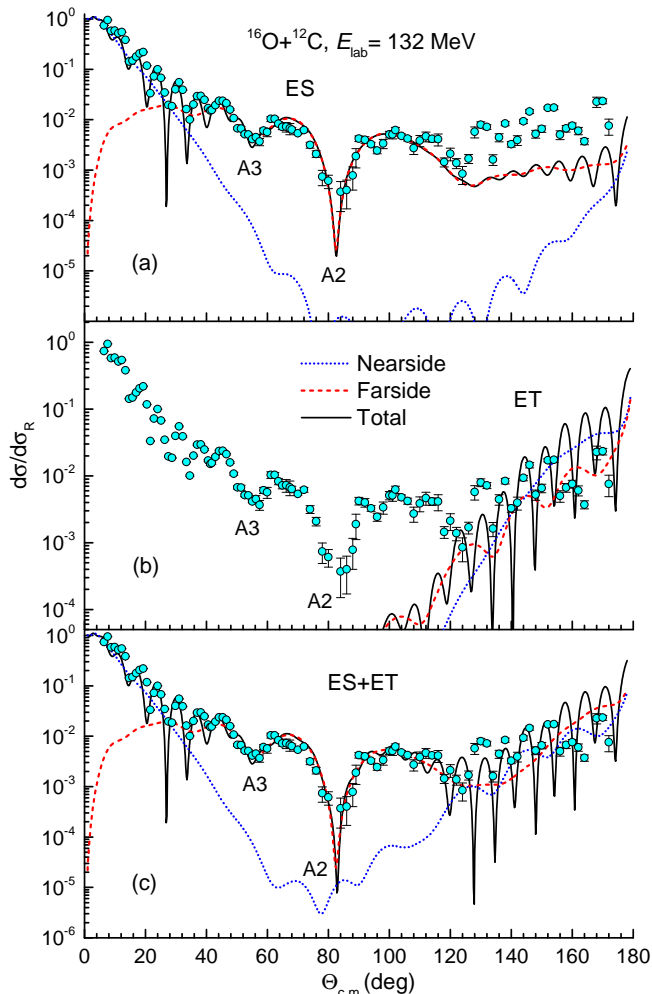


FIG. 10. NF decomposition of the elastic  $^{16}\text{O}+^{12}\text{C}$  amplitude at  $E_{\text{lab}} = 132$  MeV given by the two-channel CRC calculation using the same OP as that used in panel (b) of Fig. 9, (a) - for the purely elastic scattering (ES) only, (b) - for the elastic  $\alpha$  transfer (ET) only, and (c) - for the total (ES+ET) elastic amplitude.

$^{16}\text{O}+^{12}\text{C}$  amplitude behave in a manner similar to that shown above for the identical  $^{12}\text{C}+^{12}\text{C}$  and  $^{16}\text{O}+^{16}\text{O}$  systems. Namely,

$$f_{\text{total}}^{(\text{N})}(\theta) = f_{\text{ES}}^{(\text{N})}(\theta) + f_{\text{ET}}^{(\text{F})}(\pi - \theta), \quad (23)$$

$$f_{\text{total}}^{(\text{F})}(\theta) = f_{\text{ES}}^{(\text{F})}(\theta) + f_{\text{ET}}^{(\text{N})}(\pi - \theta). \quad (24)$$

Like the total ES amplitude of two identical nuclei (16)-(17), the nearside component (23) of the total elastic  $^{16}\text{O}+^{12}\text{C}$  amplitude is a superposition of the nearside and farside components of the ES and ET amplitudes determined at angles  $\theta$  and  $\pi - \theta$ , respectively, and vice versa for the farside component (24) of the total elastic amplitude. At the most backward angles, the ET pro-

cess become dominant and the *nearside* component of the total elastic amplitude is determined entirely by the *farside* component of the ET amplitude, and vice versa for the farside component of the total scattering amplitude, as shown in panels (b) and (c) of Fig. 10. Although the NF pattern is not symmetric as found for the elastic scattering of two identical nuclei, the NF interchange between the total elastic and ET amplitudes is naturally caused by the ET between two identical  $^{12}\text{C}$  cores, i.e., the core-core exchange symmetry of the  $^{16}\text{O}+^{12}\text{C}$  system.

## V. SUMMARY

The Fuller method of the NF decomposition of the nucleus-nucleus elastic scattering amplitude [10] has been generalized for two identical (spin-zero) nuclei, with the projectile-target exchange symmetry taken exactly into account. It is shown that the exchange symmetry of two identical nuclei results in the symmetric interchange of the nearside and farside scattering cross sections at angles passing through  $\theta = 90^\circ$ . As a result, the Airy pattern of the nuclear rainbow is reflected symmetrically about  $\theta = 90^\circ$ , and each Airy minimum located in the (direct) farside cross section at angle  $\theta < 90^\circ$  has its symmetric partner located in the (exchange) farside cross section at angle  $\pi - \theta$ .

The Mott interference pattern observed for the identical  $^{12}\text{C}+^{12}\text{C}$  and  $^{16}\text{O}+^{16}\text{O}$  systems at medium angles was found to be an interference of two farside (direct and exchange) scattering amplitudes, which results in an increased sensitivity of elastic scattering cross section around  $\theta \approx 90^\circ$  to the real OP at sub-surface distances. Therefore, elastic  $^{12}\text{C}+^{12}\text{C}$  and  $^{16}\text{O}+^{16}\text{O}$  scattering data measured at low energies [23, 26, 27] can serve as helpful probes of different theoretical models of the OP for these identical systems. Moreover, our extended NF decomposition allows for more accurate NF analyses of identical particle scattering at low energies [49], where nearside and farside amplitudes are comparable.

A similar NF interchange of the total elastic and elastic  $\alpha$  transfer amplitudes was found in the nonidentical  $^{16}\text{O}+^{12}\text{C}$  system with the core-core symmetry, where the ET process becomes dominant at backwards angles. At variance with the pure elastic scattering, a significant *non-refractive* farside component of the ET cross section was found, which indicates the surface character of the  $\alpha$  transfer between two  $^{12}\text{C}$  cores.

## ACKNOWLEDGMENTS

The present research has been supported, in part, by the National Foundation for Science and Technology Development of Vietnam (NAFOSTED Project No. 103.04-2021.74).

- 
- [1] G.R. Satchler and W.G. Love, Phys. Rep. **55**, 183 (1979).
- [2] M.E. Brandan and G.R. Satchler, Phys. Rep. **285**, 143 (1997).
- [3] D.T. Khoa, W. von Oertzen, H.G. Bohlen, and S. Ohkubo, J. Phys. G **34**, R111 (2007).
- [4] H.M. Nussenzweig, Sci. Am. **236**, 116 (1977).
- [5] M.S. Hussein and K.W. McVoy, Prog. Part. Nucl. Phys. **12**, 103 (1984).
- [6] M.E. Brandan, M.S. Hussein, K.W. McVoy, and G.R. Satchler, *Comments on nuclear and particle physics*, Vol. 22 (Gordon and Breach, New York, 1996), p. 77.
- [7] S.H. Fricke, M.E. Brandan, and K.W. McVoy, Phys. Rev. C **38**, 682 (1988).
- [8] D.M. Brink and N. Takigawa, Nucl. Phys. A **279**, 159 (1977).
- [9] N. Rowley, H. Doubre, and C. Marty, Phys. Lett. B **69**, 147 (1977).
- [10] R.C. Fuller, Phys. Rev. C **12**, 1561 (1975).
- [11] K.W. McVoy, H.M. Khalil, M.M. Shalaby, and G.R. Satchler, Nucl. Phys. A **455**, 118 (1986).
- [12] P. Fröbrich and R. Lipperheide, *Theory of Nuclear Reactions* (Clarendon, Oxford, 1996).
- [13] M.E. Brandan and G.R. Satchler, Nucl. Phys. A **487**, 477 (1988).
- [14] K.W. McVoy and M.E. Brandan, Nucl. Phys. A **542**, 295 (1992).
- [15] D.T. Khoa, W. von Oertzen, and H.G. Bohlen, Phys. Rev. C **49**, 1652 (1994).
- [16] D.T. Khoa, G.R. Satchler, and W. von Oertzen, Phys. Rev. C **56**, 954 (1997).
- [17] D.T. Khoa, W. von Oertzen, H.G. Bohlen, and F. Nuoffer, Nucl. Phys. A **672**, 387 (2000).
- [18] D.T. Khoa, N.H. Phuc, D.T. Loan, and B.M. Loc, Phys. Rev. C **94**, 034612 (2016).
- [19] G.R. Satchler, *Direct Nuclear Reactions* (Clarendon, Oxford, 1983).
- [20] J. Raynal, *Computing as a Language of Physics* (IAEA, Vienna, 1972) p. 75; J. Raynal, coupled-channel code ECIS97 (unpublished).
- [21] I.J. Thompson, Comput. Phys. Rep. **7**, 167 (1988); <http://www.fresco.org.uk>.
- [22] I.J. Thompson and F.M. Nunes, *Nuclear Reactions for Astrophysics* (Cambridge University Press, Cambridge, UK, 2009).
- [23] R.G. Stokstad, R.M. Wieland, G.R. Satchler, C.B. Fulmer, D.C. Hensley, S. Raman, L.D. Rickertsen, A.H. Snell, and P.H. Stelson, Phys. Rev. C **20**, 655 (1979).
- [24] E. Stiliaris, H. G. Bohlen, P. Fröbrich, B. Gebauer, D. Kolbert, W. von Oertzen, M. Wilpert, and Th. Wilpert, Phys. Lett. B **223**, 291 (1989).
- [25] D.T. Khoa, W. von Oertzen, H. G. Bohlen, G. Bartnitzky, H. Clement, Y. Sugiyama, B. Gebauer, A.N. Ostrowski, Th. Wilpert, M. Wilpert, and C. Langner, Phys. Rev. Lett. **74**, 34 (1995).
- [26] Y. Sugiyama *et al.*, Phys. Lett. B **312**, 35 (1993).
- [27] Y. Kondo *et al.*, Phys. Lett. B **365**, 17 (1996).
- [28] L.H. Chien, D.T. Khoa, D.C. Cuong, and N.H. Phuc, Phys. Rev. C **98**, 064604 (2018).
- [29] M.E. Brandan and G.R. Satchler, Phys. Lett. B **256**, 311 (1991).
- [30] M. E. Brandan, A. Menchaca-Rocha, L. Trache, H.L. Clark, A. Azhari, C. A. Gagliardi, Y.-W. Lui, R. E. Tribble, R. L. Varner, J. R. Beene, and G. R. Satchler, Nucl. Phys. A **688**, 659 (2001).
- [31] A.A. Ogloblin, D.T. Khoa, Y. Kondō, Yu.A. Glukhov, A.S. Demyanova, M.V. Rozhkov, G.R. Satchler, and S.A. Goncharov, Phys. Rev. C **57**, 1797 (1998).
- [32] A.A. Ogloblin, Yu.A. Glukhov, W.H. Trzaska, A.S. Demyanova, S.A. Goncharov, R. Julin, S.V. Klebnikov, M. Mutterer, M.V. Rozhkov, V.P. Rudakov, G.P. Tiorin, D.T. Khoa, and G.R. Satchler, Phys. Rev. C **62**, 044601 (2000).
- [33] Yu. A. Glukhov, S.A. Goncharov, A.S. Demyanova, A.A. Ogloblin, M.V. Rozhkov, V.P. Rudakov, and V. Trashka, Izv. Ross. Akad. Nauk, Ser. Fiz. **65**, 647 (2001).
- [34] Yu. A. Glukhov, V. P. Rudakov, K. P. Artemov, A. S. Demyanova, A. A. Ogloblin, S. A. Goncharov, and A. Izadpanakh, Phys. At. Nucl. **70**, 1 (2007).
- [35] M.P. Nicoli, F. Haas, R.M. Freeman, S. Szilner, Z. Basrak, A. Morsad, G.R. Satchler, and M. E. Brandan, Phys. Rev. C **61**, 034609 (2000).
- [36] S. Szilner, W. von Oertzen, Z. Basrak, F. Haas, and M. Milin, Eur. Phys. J. A **13**, 273 (2002).
- [37] A.T. Rudchik *et al.*, Eur. Phys. J. A **44**, 221 (2010).
- [38] N.T.T. Phuc, N.H. Phuc, and D.T. Khoa, Phys. Rev. C **98**, 024613 (2018).
- [39] N.H. Phuc, D.T. Khoa, and N.T.T. Phuc, Eur. Phys. J. A **57**, 7 (2021).
- [40] J.L. Ferreira, J. Lubian, R. Linares, M.J. Ermamatov, H. Yépez-Martínez, and P.O. Hess, Eur. Phys. J. A **55**, 94 (2019).
- [41] W. von Oertzen and H.G. Bohlen, Phys. Rep. **19**, 1 (1975).
- [42] W.E. Frahn and M.S. Hussein, Nucl. Phys. A **346**, 237 (1980).
- [43] W.E. Frahn and M.S. Hussein, Phys. Lett. **90B**, 358 (1980).
- [44] N.T.T. Phuc, R.S. Mackintosh, N.H. Phuc, and D.T. Khoa, Phys. Rev. C **100**, 054615 (2019).
- [45] M.C. Morais and R. Lichtenthäler, Nucl. Phys. A **857**, 1 (2011).
- [46] A. Volya and Y. M. Tchuvisky, Phys. Rev. C **91**, 044319 (2015).
- [47] T. Yamada, Y. Funaki, T. Myo, H. Horiuchi, K. Ikeda, G. Röpke, P. Schuck, and A. Tohsaki, Phys. Rev. C **85**, 034315 (2012).
- [48] J. Dohet-Eraly and P. Descouvemont, Phys. Rev. C **103**, 034619 (2021).
- [49] K. Hagino and T. Yoda, Phys. Lett. B **848**, 138326 (2024).